Reconstructing extreme climatic and geochemical conditions during the largest natural mangrove dieback on record

James Z. Sippo[1,2], Isaac R. Santos[2,3], Christian J. Sanders[2], Patricia Gadd[4], Quan Hua[4], Catherine E. Lovelock[5], Nadia S. Santini[6,7], Scott G. Johnston[1], Yota Harada[8], Gloria Reithmeir[1], Damien T. Maher[1,9]

[1]Southern Cross Geoscience, Southern Cross University, Lismore, 2480 Australia.
[2]National Marine Science Centre, Southern Cross University, PO Box 4321, Coffs Harbour, NSW 2450, Australia
[3]Department of Marine Sciences, University of Gothenburg, Sweden
[4]Australian Nuclear Science and Technology Organisation (ANSTO), Locked Bag 2001, Kirrawee DC, NSW 2232, Australia
[5]School of Biological Sciences, the University of Queensland, St Lucia QLD 4072, Australia
[6]Cátedra Consejo Nacional de Ciencia y Tecnología, Av. Insurgentes Sur 1582, Crédito Constructor, Benito Juárez, 03940, Ciudad de México, Mexico.
[7]Instituto de Ecología, Universidad Nacional Autónoma de México, Ciudad Universitaria, 04500, Ciudad de México, Mexico.
[8]Australian Rivers Institute – Coast and Estuaries, and School of Environment and Science, Griffith University, Gold Coast, QLD 4222, Australia
[9]School of Environment, Science and Engineering, Southern Cross University, Lismore 2480, Australia

Abstract

A massive mangrove dieback event occurred in 2015/2016 along ~1000km of pristine coastline in the Gulf of Carpentaria, Australia. Here, we use sediment and wood chronologies to gain insights into geochemical and climatic changes related to this dieback. The unique combination of low rainfall and low sea level observed during the dieback event was unprecedented in the previous three decades. A combination of iron (Fe) chronologies in wood and sediment, wood density and estimates of mangrove water use efficiency, all imply lower water availability within the dead mangrove forest. Wood and sediment chronologies suggest a rapid, large mobilization of sedimentary Fe, which is consistent with redox transitions promoted by changes in soil moisture content. Elemental analysis of wood cross sections revealed 30-90 fold increase in Fe concentrations in dead mangroves just prior to their mortality. Mangrove wood uptake of Fe during the dieback is consistent with large apparent losses of Fe from sediments, which potentially caused an outwelling of Fe to the ocean. Although Fe toxicity may also have played a role in the dieback, this possibility requires further study. We suggest that differences in wood and sedimentary Fe between living and dead forest areas reflect sediment redox transitions that are in turn associated with regional variability in groundwater flows. Overall, our observations provide multiple lines of evidence that the forest dieback was associated with low water availability, coinciding with a strong ENSO event.

Introduction

Mangroves provide a wide range of ecosystem services, including nursery habitat, carbon sequestration, and coastal protection (Barbier et al. 2011, Donato et al. 2011). Climate change is a major threat to mangroves, which adds to existing stressors imposed by deforestation and over-exploitation (Hamilton and Casey 2016, Richards and Friess 2016). Sea level rise, altered sediment budgets, reduced water availability and increasing climatic extremes are all negatively affecting mangroves (Gilman et al. 2008, Alongi 2015, Lovelock et al. 2015, Sippo et al. 2018).

In Australia, an extensive mangrove dieback event in the Gulf of Carpentaria during December 2015 - January 2016, coincided with extreme drought and low regional sea levels. This extreme climatic event drove the largest recorded mangrove mortality event (~1000 km coastline, ~7400 ha) attributed to natural causes (Duke et al., 2017; Harris et al., 2017; Sippo et al., 2018) and led to extensive changes in the coastal carbon cycle (Sippo et al. 2019; Sippo et al. 2020) and coastal foodwebs (Harada et al. 2020). Two other large scale mangrove dieback events occurred at the same time, one in Exmouth (Lovelock et al. 2017) and the other in Kakadu National Park, Australia (Asbridge et al. 2019).

Mangrove mortality has been previously attributed to low water availability associated with extreme drought. Limited rainfall and groundwater availability combined with anomalously low sea levels, effectively reduced tidal inundation and soil water content (Duke et al., 2017; Harris et al., 2017). A strong El Niño event resulted in the lowest recorded rainfall in the nine months preceding the mangrove dieback since 1971, and was accompanied by regional sea levels that were 20 cm lower than average (Harris et al., 2017). Atmospheric moisture was also unusually low during 2015 - a feature which may influence the physiological functioning of mangrove trees (Nguyen et al. 2017). Such severe climatic and hydrologic changes may affect both plant physiology and sediment geochemistry.

In contrast to terrestrial forest soils, mangrove sediments are largely anoxic due to their water-logged nature, and high organic matter contents. Mangrove sediments also receive a supply of materials from both terrestrial environments (e.g. Fe, sediments) and oceanic water (e.g. SO_4) which results in distinctly different biogeochemical cycling than terrestrial forests (Burdige 2011). As a result, mangrove sediments often accumulate substantial (~1-5%) bioauthigenic pyrite (FeS_2). Pyrite remains stable under waterlogged and reducing conditions (van Breemen 1988, Johnston et al. 2011). However, lowering of water levels can alter sediment redox conditions and result in rapid oxidation of FeS_2, releasing acid and dissolved Fe (mostly as more soluble Fe^{2+} species) to porewaters (Burton et al. 2006, Johnston et al. 2011, Keene et al. 2014). Subsequent oxidation of Fe^{2+} and precipitation of Fe(III) (oxy)hydroxide minerals can then lead to the accumulation of highly reactive Fe in sediments. Such reactive Fe(III) minerals are in turn readily subject to reductive dissolution and (re)-formation of soluble Fe^{2+} species during any subsequent switch to more reducing conditions. Thus, changes in sediment redox conditions (e.g. increased oxidation and followed by subsequent reduction), in mangrove sediments that are rich in FeS_2 can cause a release of relatively mobile and bioavailable Fe^{2+} during the redox transition(s).

Mobilisation of Fe due to fluctuating oxidation/reduction cycles could also have important consequences for coastal Fe cycling. For example, Fe is often a limiting nutrient in ocean surface waters and thus Fe outwelling from mangroves could have important implications for primary productivity in coastal zone waters (Jickells and Spokes , Fung et al. 2000, Holloway

et al. 2016). Fe mobilisation also means that uptake of Fe^{2+} into mangrove tissues may be a powerful proxy for historic sediment redox conditions. However, the process of Fe assimilation into mangrove tissues remains poorly understood. Marchand et al. (2016) suggest that the presence of Fe^{2+} may result in an increased Fe uptake by the root system. Such uptake may be toxic for the plant by reducing photosynthesis, increasing oxidative stress, and damaging membranes, DNA and proteins (Marchand et al., 2016). Fe toxicity in some mangrove species is reported to occur at concentrations ~2 fold higher than the optimal Fe supply for maximal growth (Alongi, 2010). However, to our knowledge, Fe toxicity in *Avicenia marina* at extremely high Fe concentrations has not been investigated.

An extensive saltmarsh dieback in southern United States in 2000 provides an analogue to the mangrove dieback studied here. The saltmarsh dieback coincided with severe drought conditions (McKee et al. 2004, Ogburn and Alber 2006, Alber et al. 2008). McKee et al. (2004) found that sediments in dead saltmarsh areas had significantly higher acidity upon oxidation than alive areas. The dieback may have been caused by a combination of reduced water availability, increased sediment salinities and/or metal toxicity associated with soil acidification following sediment pyrite oxidation. However, the precise cause of the dieback is a matter of debate and remains inconclusive (McKee et al. 2004, Silliman et al. 2005, Alber et al. 2008). In contrast to the herbaceous salt marsh species affected in the US dieback, mangroves are woody - thus providing opportunity for dendrochronological climatic reconstruction (Verheyden et al. 2005, Brookhouse 2006). To date, the use of dendrochronological techniques have not been used to assess changes in sediment geochemistry in mangroves.

Here, we combine multiple wood and sediment chronology techniques to reconstruct water availability, sediment geochemistry and assess the links to climate and sea levels. To evaluate the potential for mobilisation of Fe during the dieback, we combine multiple lines of evidence including: 1) micro X-ray fluorescence (Itrax) to analyse the elemental composition in wood and sediment cores; 2) wood density measurements, tree growth rates and $\delta^{13}C$ isotopes to assess historic changes in water availability (Santini et al. 2012, Santini et al. 2013, Van Der Sleen et al. 2015, Maxwell et al. 2018); and 3) sediment profiles of FeS_2 concentrations to provide insight into sediment redox conditions and possible Fe mobilisation. We assess these parameters in areas where mangroves died and where they survived the dieback event.

Methods

Study Site

This study was conducted in the South Eastern corner of the Gulf of Carpentaria, in Northern Australia (Figure 1). The Gulf of Carpentaria is a large and shallow (< 70 m) waterbody with an annual rainfall of 900mm per year and a semi-arid climate (Bureau of Meteorology; Duke et al., 2017). The region has low lying topography with *A. marina* and *Rhizophora stylosa* the dominant mangroves fringing the coastline and estuaries, and extensive saltpans in the upper intertidal zone (Duke et al., 2017). Widespread dieback of the mangroves in the region was observed in 2015-2016.

The dieback predominantly affected *A. marina* which occupy the open coastlines and upper intertidal areas (Duke et al., 2017). Although 7500 ha of mangrove suffered mortality some areas remained relatively unaffected, providing an opportunity to compare conditions within

live and dead stands. We assessed a live and dead mangrove area 20 months after the dieback event. The two mangrove areas were separated by the Norman River and were ~4 km apart (Figure 1). The living mangrove has an area of 175 ha and had some dead trees in the upper intertidal zone and living trees that showed signs of stress (dead branches and partial defoliation). Towards the seaward edge, the forest had no signs of canopy loss 8 months post dieback event. The dead mangrove area was 169 ha and had close to 100% mortality (Figure 1b), with only some trees at the waterline showing regrowth.

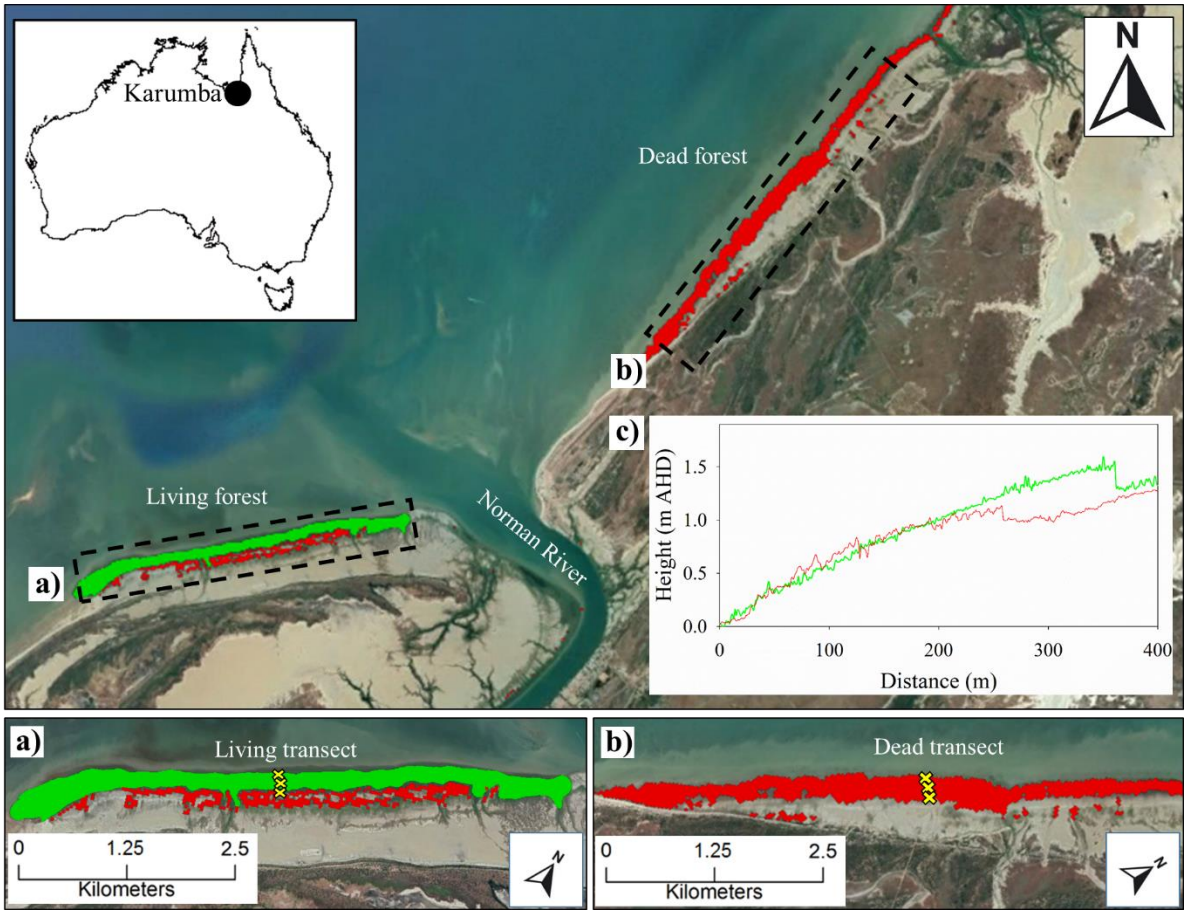

Figure 1. Study sites of a) living mangrove area (green) and b) dead mangrove area (red) near the mouth of the Norman River, Karumba Qld. Note: The yellow 'x' symbols represent transects through the upper, middle and lower study sites. c) Elevation above the Australian Height Datum (AHD) from Lidar DEM were measured from the seaward mangrove edge in 2017 from the same transects as samples were collected in 2016 through the living (Green line) and dead (red line) mangrove area (data available from http://wiki.auscover.net.au/wiki/Mangroves). Satellite images sourced from © Google Earth (2019) and Queensland Government (2019).

Field sampling and chemical and isotopic analyses

Tree and sediment samples were collected in August 2017 approximately 20 months after the dieback event. Wood and sediment samples were collected from transects from the lower intertidal zone to the upper intertidal zone (Figure 1). Fully mature trees were selected at ~20 m inward from the lower and upper intertidal forest edges and in the centre of the forest. One upper, mid and lower tide wood sample was taken in living and dead mangrove areas (Figure 1a and b). Wood samples from *A. marina* were taken from 50 cm above ground level by cutting a 1cm thick disk from the trunk. At the upper and lower intertidal sites, two sediment cores were taken. One core, taken to 2 m with a Russian peat auger with extensions, was

sampled for elemental analysis with Itrax. A second core, taken to a depth of 1 m using a tapered auger corer in August 2018 at the same site, was sampled for analysis of chromium reducible sulfur (CRS).

Wood samples were dated using bomb ^{14}C (eg, Santini et al. 2013; Witt et al. 2017). Water-use efficiency (WUE), which is the ratio of net photosynthesis to transpiration, was assessed using wood cellulose stable isotopic composition $\delta^{13}C$ following Van Der Sleen et al., (2015) as water use efficiency correlates with $\delta^{13}C$ (Farquhar and Richards 1984, Farquhar et al. 1989). Sub-samples for ^{14}C and $\delta^{13}C$ were taken from tree samples (wood disks) along the longest radius of each disk at regular intervals from the centre to the outer edge (youngest wood). The sub-samples were collected using a scalpel parallel to tree rings to reduce errors. Alpha cellulose was extracted from the wooden sub-samples (Hua et al., 2004b), combusted to CO_2 and converted to graphite (Hua et al., 2001). A portion of graphite was used for the determination of $\delta^{13}C$ for isotopic fractionation correction using a Micromass IsoPrime elemental analyser/isotope ratio mass spectrometer (EA/IRMS) at the Australian Nuclear Science and Technology Organisation (ANSTO). The remaining graphite was analysed for ^{14}C using the STAR accelerator mass spectrometry (AMS) facility at ANSTO (Fink et al. 2004) with a typical analytical precision of better than 0.3% (2σ). Oxalic acid I (HOxI) was used as the primary standard for calculating sample ^{14}C content, while oxalic acid II (HOxII) and IAEA-C7 reference material were used as check standards. Sample ^{14}C content was converted to calendar ages using the ‘‘Simple Sequence’’ deposition model of the OxCal calibration program based on chronological ordering (outer samples are younger than inner samples) (Bronk Ramsey, 2008), and atmospheric ^{14}C data from Baring Head (Wellington, New Zealand) extended to 2017.

Wood samples and sediment cores were analysed for elemental composition with a micro X-ray fluorescence conducted at ANSTO using an Itrax core scanner (Cox Analytical Systems). The scanner produces a high resolution (0.2 mm) radiographic density pattern and semi-quantitative elemental profiles for each sample. The Itrax measured 34 elements and while trends occurred in some elements (see Appendix 1 & 2), here we focus on Fe. Itrax Fe results have been compared with absolute Fe_2O_3 concentrations with high accuracy ($R^2 = 0.74$) (Hunt et al., 2015). Wood samples were scanned along the same transect as for ^{14}C samples, i.e. the longest radius from the wood core to the outer edge. Sediment cores were analysed using the Itrax in four 50 cm increments. Immediately upon collection, CRS sub-samples were placed in polyethylene bags with air removed and frozen prior to CRS analysis. Chromium reducible sulfur (CRS) was measured at 5 cm intervals to 1 m depth to provide an estimate of reducible inorganic S (RIS) species such as pyrite (FeS_2 - a key oxygen-sensitive sedimentary Fe species) with a linear relationship of $R^2 = 0.996$ (Burton et al., 2008). Groundwater salinity values were taken at the same sites as wood samples from bore holes dug to ~1m depth. Groundwater in the holes was purged and allowed to refill and salinities were measured using a Hach multi-sonde.

Data analysis

To align radiocarbon calendar ages with Itrax data, we interpolated ages using the wood circumference. Itrax elemental and density data were normalized as the mean subtracted from each value divided by the standard deviation following Hevia et al. (2018) and are referred to hereforth as relative concentrations. We also normalized the Fe data to total counts and other measured elements following Turner et al. (2015) and Gregory et al. (2019) to confirm the trends did not change with different normalization approaches which they did not. This

normalization reduces external effects (Gregory et al. 2019) and allows a more direct comparison between samples from living and dead forest areas. Methods that provided absolute concentrations such as CRS are simply referred to as concentrations. Growth rates in mm per year were calculated as the measured increment divided by the difference in years (estimated from ^{14}C) between samples. De-trended growth rates were then calculated as the deviation from the exponential curve fitted to growth rates for each sample. Water use efficiency (WUE) was calculated from $\delta^{13}C$ isotope values (Van Der Sleen et al. 2015). Differences in WUE between living and dead mangrove areas were compared using T-test.

Cross correlations with a time lag of one-month intervals were used to evaluate the relationships between climatic variables (the Southern Oscillation Index (SOI), sea level, rainfall and vapour pressure) with wood density, elemental relative concentrations and growth rates. SOI data and other climate data were obtained from the Bureau of Meteorology (Station number 029028, 2019) and published reports (Jones et al. 2009, Harris et al. 2017). All climatic data were used with a one month resolution and were smoothed using a centred moving mean. This time lag analysis was specifically chosen to examine relationships between climate variables and Fe over a two year period because records of all climate variables are in resolution of months, but the chronology of Fe (based on ^{14}C dates) is in years.

Results

Climatic conditions

The climate records over the last three decades reveal an unprecedented combination of low sea level and low annual rainfall. SOI is significantly correlated to all climate variables (Pearson product moment correlation, $P < 0.05$). Lower sea levels and rainfall had previously occurred independently (Figure 2). Since 1985, trends in SOI index based on vapour pressure, precipitation and sea level observations show El Niño in 1983, 1987, 1992, 1994, 1998, 2015 and 2016.

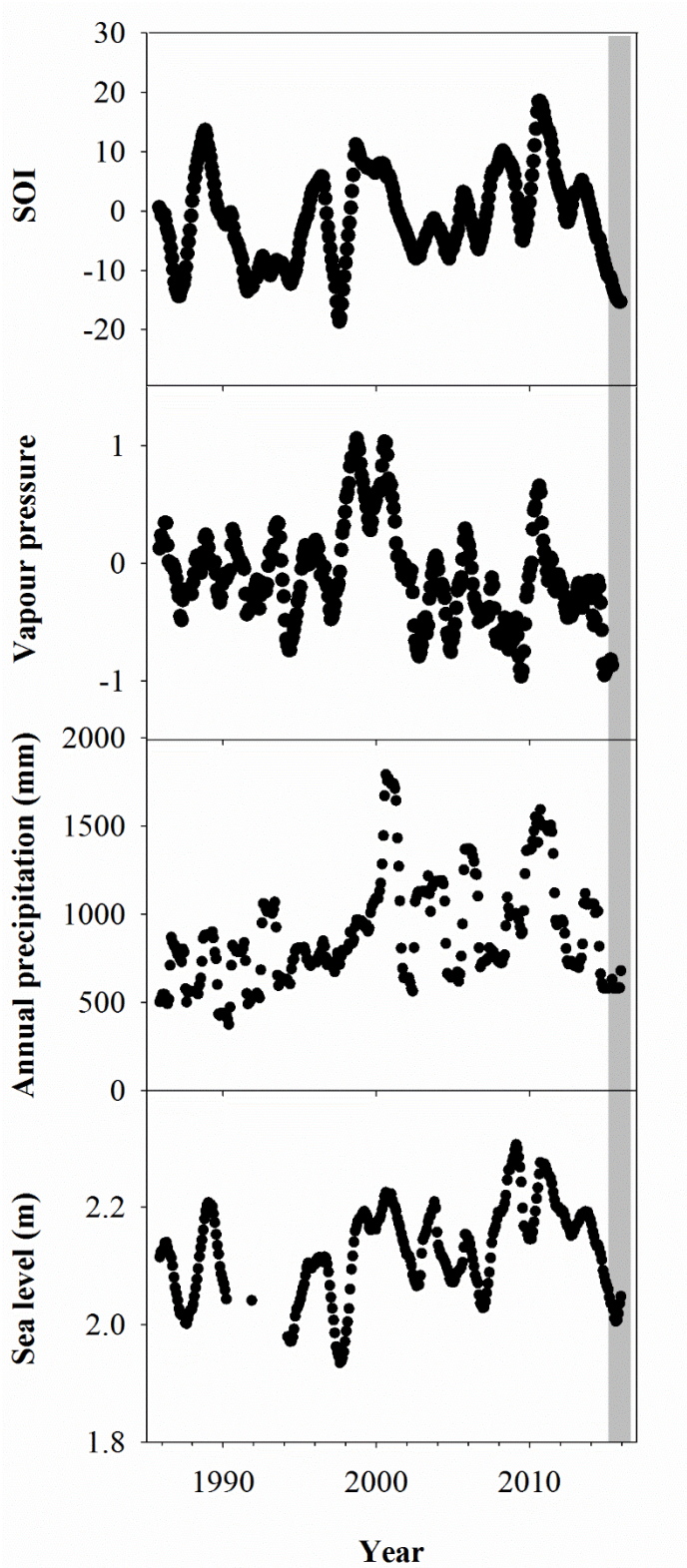

Figure 2. Climate observations from the South Eastern Gulf of Carpentaria Australian (Jones et al. 2009, Harris et al. 2017, Bureau of Meteorology 2019). The grey bar represents the period during which the dieback event occurred.

Wood samples and ages

The ages of *A. marina* ranged from 15 ± 2 to 34 ± 2 years (Table 1). On average, the trees in the living and dead mangrove forests were 21 ± 4 and 34 ± 1 years old respectively. Tree growth rates that were de-trended to negative exponential growth had no trends over time in either the living or dead mangrove areas (Table 1).

Table 1. Summary of radiocarbon ages and growth rates (deviation from negative exponential growth) for all wood samples taken from dead and living mangrove areas in the Gulf of Carpentaria, Australia.

Sample	Distance from pith (mm)	^{14}C Mean ±1σ (pMC) **	Modelled calendar age Mean ±1σ (year AD)	Deviation from negative exponential growth (mm per year)
		Dead mangrove		
Upper intertidal	2	121.98 ± 0.28	1984 ± 2	-
	17	119.82 ± 0.27	1986 ± 2	-2.6
	35	118.02 ± 0.27	1988 ± 2	-1.4
	52	116.07 ± 0.30	1990 ± 3	-1.2
	70	110.85 ± 0.26	1998 ± 2	-4.7
	87	105.35 ± 0.23	2010 ± 2	-1.3
	89		2015*	-0.9
Mid intertidal	2	123.56 ± 0.30	1983 ± 2	-
	12	122.81 ± 0.30	1984 ± 2	2.3
	24	119.07 ± 0.28	1987 ± 2	-4.8
	36	115.92 ± 0.38	1991 ± 3	-3.6
	49	110.06 ± 0.27	1999 ± 2	-3.7
	62	105.17 ± 0.29	2011 ± 3	-0.2
	64		2015*	-0.2
Lower intertidal	2	123.31 ± 0.38	1983 ± 2	-
	23	120.39 ± 0.36	1986 ± 2	-2.3
	45	117.35 ± 0.35	1989 ± 2	-1.8
	89	110.89 ± 0.33	1998 ± 2	-1.9
	110	105.75 ± 0.31	2009 ± 2	-2.1
	113		2015*	-2.5
		Living mangrove		
Upper intertidal	2	163.84 ± 0.48	1995 ± 2	-
	20	112.00 ± 0.42	1996 ± 3	2.3
	40	109.81 ± 0.44	2000 ± 3	-0.8
	58	103.71 ± 0.40	2013 ± 2	-2.3
	60		2017*	-2.9
Mid intertidal	2	113.32 ± 0.45	1994 ± 2	-
	16	111.13 ± 0.31	1997 ± 2	-1.0
	33	109.22 ± 0.37	2001 ± 2	0.8

	49	106.59	±	0.29	2014	±	2	-1.2
	50				2017*			-2.3
Mid intertidal	2	113.41	±	0.29	1993	±	3	-
	25	110.89	±	0.28	1998	±	2	-1.0
	50	101.91	±	0.30	2017	±	1	0.2
	51				2017*			-2.3
Lower intertidal	2	108.83	±	0.27	2002	±	2	-
	17	107.30	±	0.29	2005	±	2	-5.1
	33	104.92	±	0.37	2011	±	3	9.2
	46	104.30	±	0.34	2014	±	2	-2.3
	48				2017*			-2.2

* Date of collection of *A. marina* samples
**Measured ^{14}C content is shown in percent Modern Carbon (pMC; Stuiver and Polach 1977)

Fe in wood and sediment cores

Fe relative concentrations in all dead mangrove samples peaked at the time of mangrove mortality in late 2015/early 2016 (Figure 3). In the living mangrove samples, Fe peaked in late 2015/early 2016 and then decreased in 2016 and 2017 to long-term average levels. Peak wood Fe concentrations in the upper, mid and lower intertidal areas of the dead mangrove samples were 40, 90 and 30 fold higher than their mean baseline concentrations, respectively. In the living mangrove area, peak wood Fe concentrations in the upper, mid and lower intertidal areas were 25, 4 and 3 fold higher than their mean baseline concentrations, respectively. In the dead mangrove area, Fe levels were similar from the upper to the lower intertidal zone (Figure 3). In the living mangrove area, Fe was highest in the upper and mid intertidal zone and decreased in the lower intertidal zone. Itrax trends are plotted against ^{14}C ages and since tree growth rates change over time, Itrax data is not evenly distributed over time.

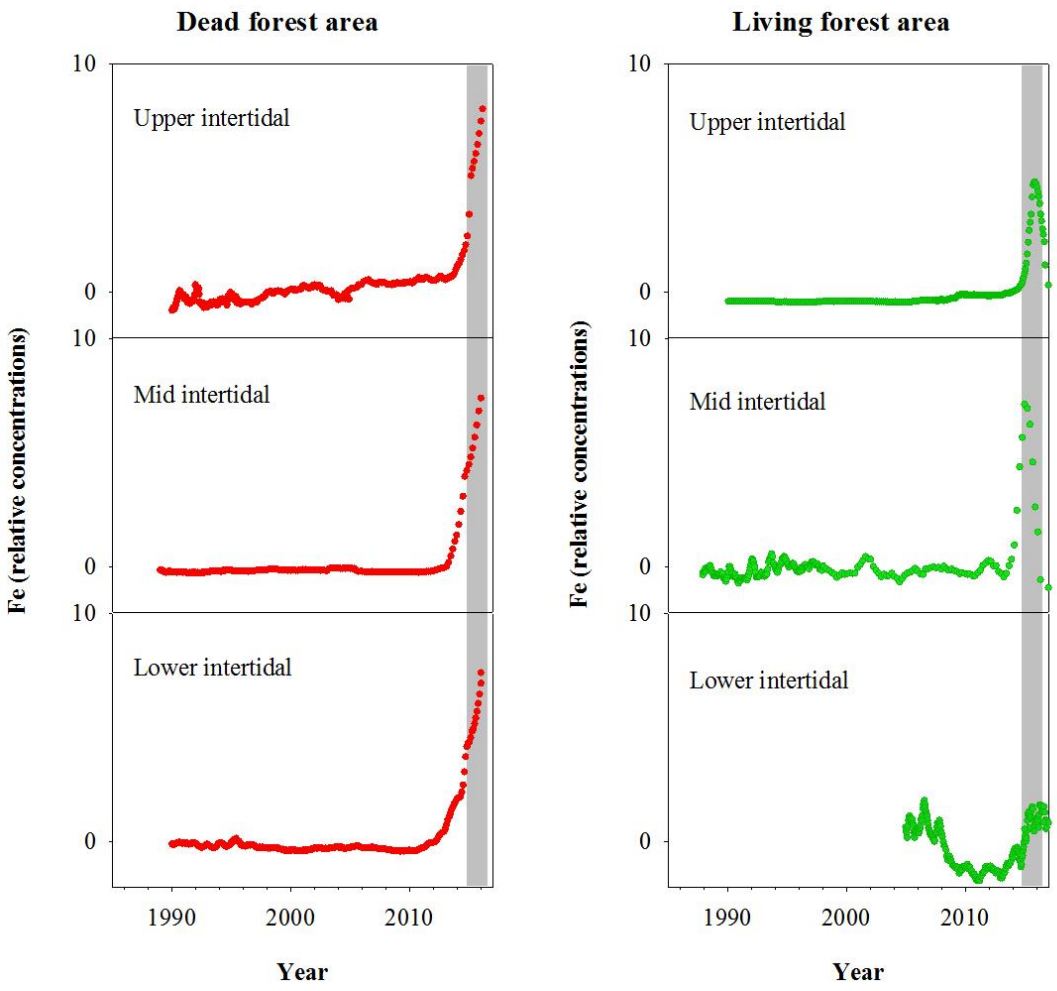

Figure 3. Fe relative concentrations in mangrove wood over time in living (green dots) and dead (red dots) from upper, mid and lower intertidal areas of mangroves of the Gulf of Carpentaria, Australia. Grey areas indicate the dieback event.

Significant correlations with no time lag were found between Fe in wood and vapour pressure, rainfall, sea level and SOI (Figure 4). All climate variables were strongly correlated with SOI. Therefore, we could not separate the influence of individual climate variables on wood Fe. In the dead and living mangrove areas, the strongest correlations with Fe occurred with no time lag (Figure 4).

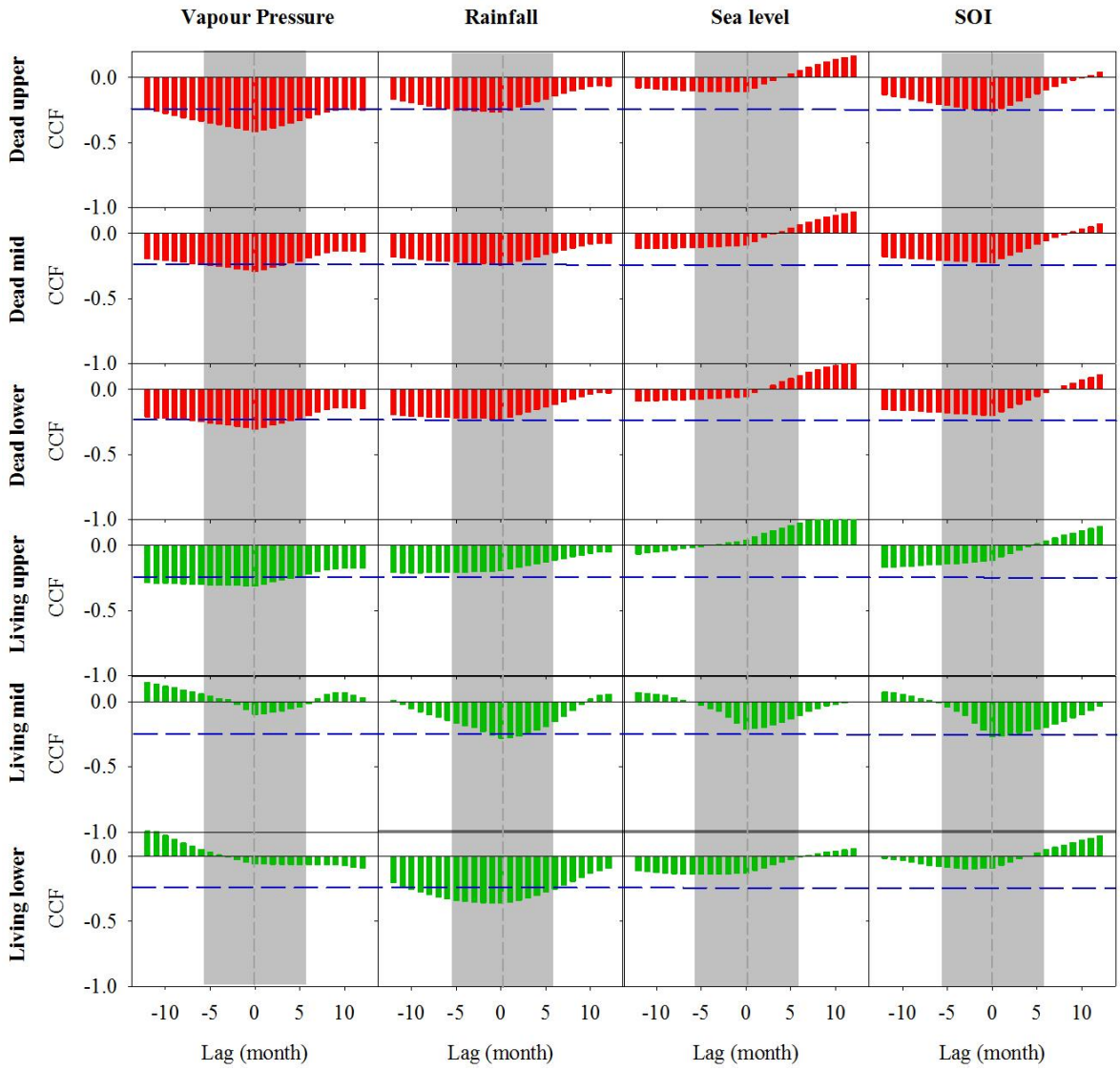

Figure 4. Cross correlation function (CCF) between Fe in wood samples and climate data at one month resolution over a 12 month period prior and post dieback. Wood samples are from the upper, mid and lower intertidal zones of the dead (red) and living (green) mangrove areas. Blue horizontal dashed lines indicate P< 0.01 with n=125. Grey dashed vertical lines at zero lag indicate dieback period and the grey bar represents the period during which the dieback event occurred.

Sediment cores had a similar pattern of decreasing Fe with depth in upper and lower intertidal areas, and in living and dead mangrove areas (Figure 5a). Dead mangrove areas were depleted in Fe by ~32% in the surface 50 cm and ~26% in the surface 1 m relative to the respective living mangrove areas in both the upper and lower intertidal area (Figure 5b, c and d). Fe relative concentrations were significantly higher in living mangrove areas compared to dead mangrove areas (Mann-Whitney Rank Sum Test, $P < 0.001$ for all depths).

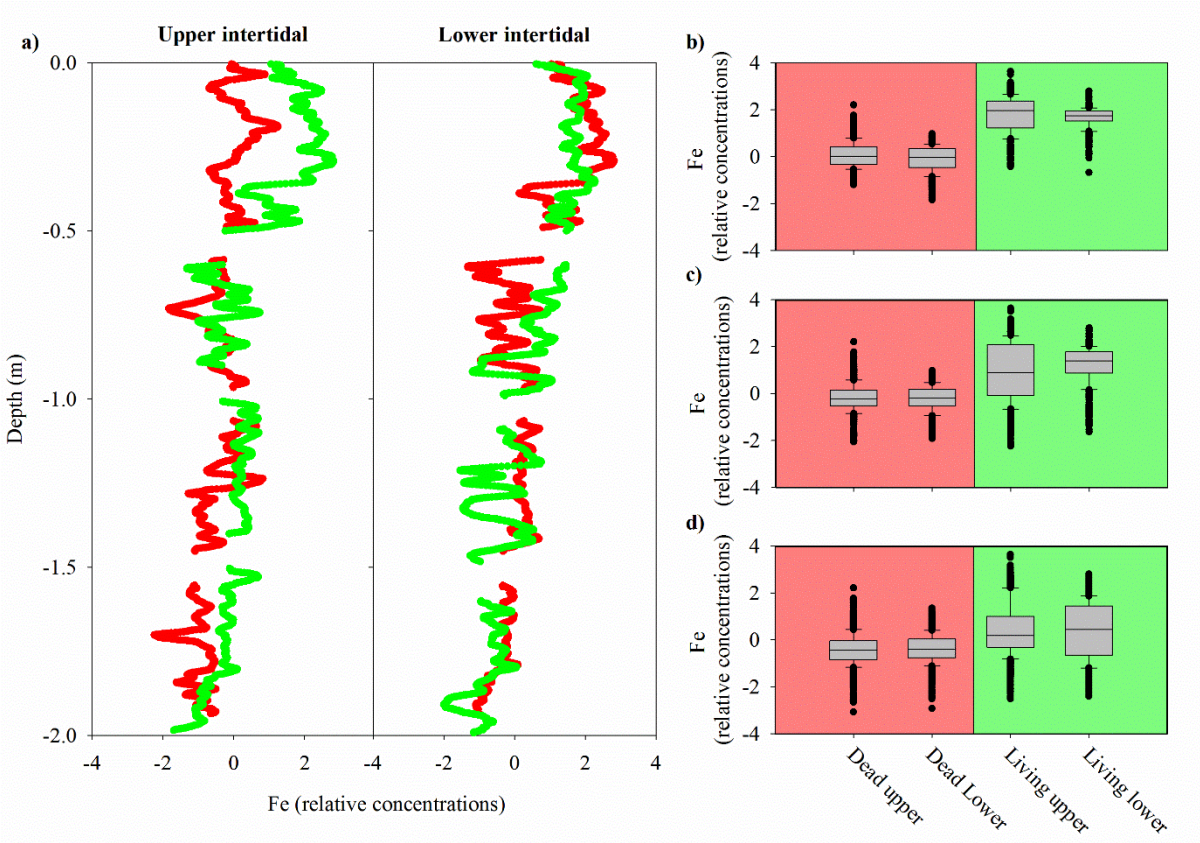

Figure 5. a) Fe relative concentrations in sediment cores to 2m depth from the upper and lower intertidal areas of living (green) and dead (red) mangroves in the Gulf of Carpentaria, based on Itrax analysis. Box plots of normalised Fe relative concentrations from sediment cores to b) 0.5 m, c) 1 m and d) 2 m depth. The central horizontal line represents the median value, the box represents the upper and lower quartiles, and the whiskers represent the maximum and minimum values excluding outliers, i.e., black dots.

Chromium Reduced Sulfur (CRS) absolute concentrations, which provide a proxy for pyrite concentrations in sediment cores, were also lower overall in the dead mangrove compared to the living mangrove area - by 36% in the upper and 38% in the lower intertidal zones respectively (Figure 6). Although these differences were not significant (Mann-Whitney Rank Sum Test, $P > 0.05$), they were very similar to Itrax Fe trends. In the upper intertidal zone, CRS concentrations generally increased with depth, while in the lower intertidal zone, CRS concentrations peaked from ~10 cm below the surface in both dead and living sediment samples and then decreased with depth. Differences in CRS concentrations (in both the upper and lower intertidal zones) between the dead and living mangroves were most prominent in the upper ~60 cm of each core and tended to converge at greater depths (Figure 6).

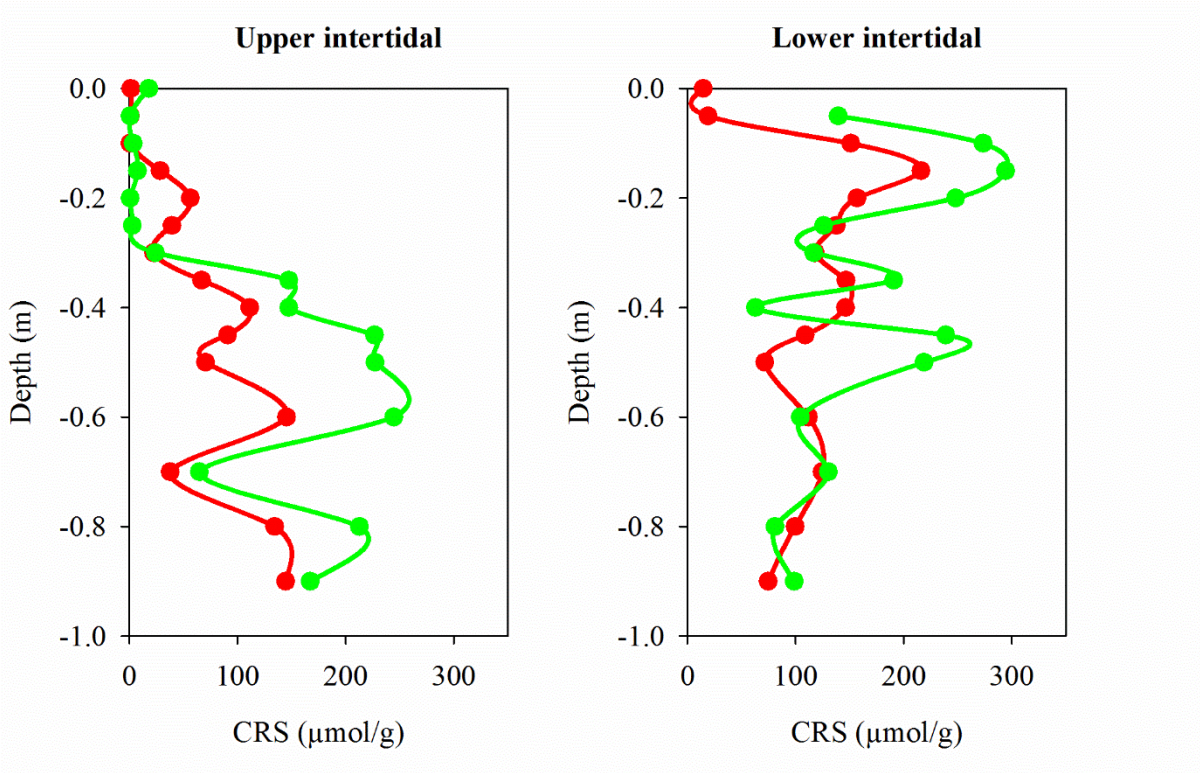

Figure 6. Chromium reducible sulfur (CRS) profiles (a proxy for pyrite) from sediment cores in dead (red) and living (green) mangrove areas in the Gulf of Carpentaria.

Water use efficiency (WUE) calculated from $\delta^{13}C$ decreased in all wood samples from 1983 to 2017 (Figure 7a), suggesting increasing water availability in the study area. During the dieback event, median WUE values were higher in dead samples than in living samples, with the differences more pronounced in the upper intertidal zones (Figure 7b). Comparison of WUE in dead and living mangrove samples suggests lower water availability in the dead mangrove area (Figure 7b). However, the mean WUE values were compared from 1983 to 2017 and were not significantly different (T-test, P = 0.2) in dead and living mangrove areas. Groundwater salinity values were highest in the upper intertidal mangrove areas and lowest in the lower intertidal areas (Figure 7c). Salinities were not significantly different in the living and dead forest areas (T-test, P = 0.913).

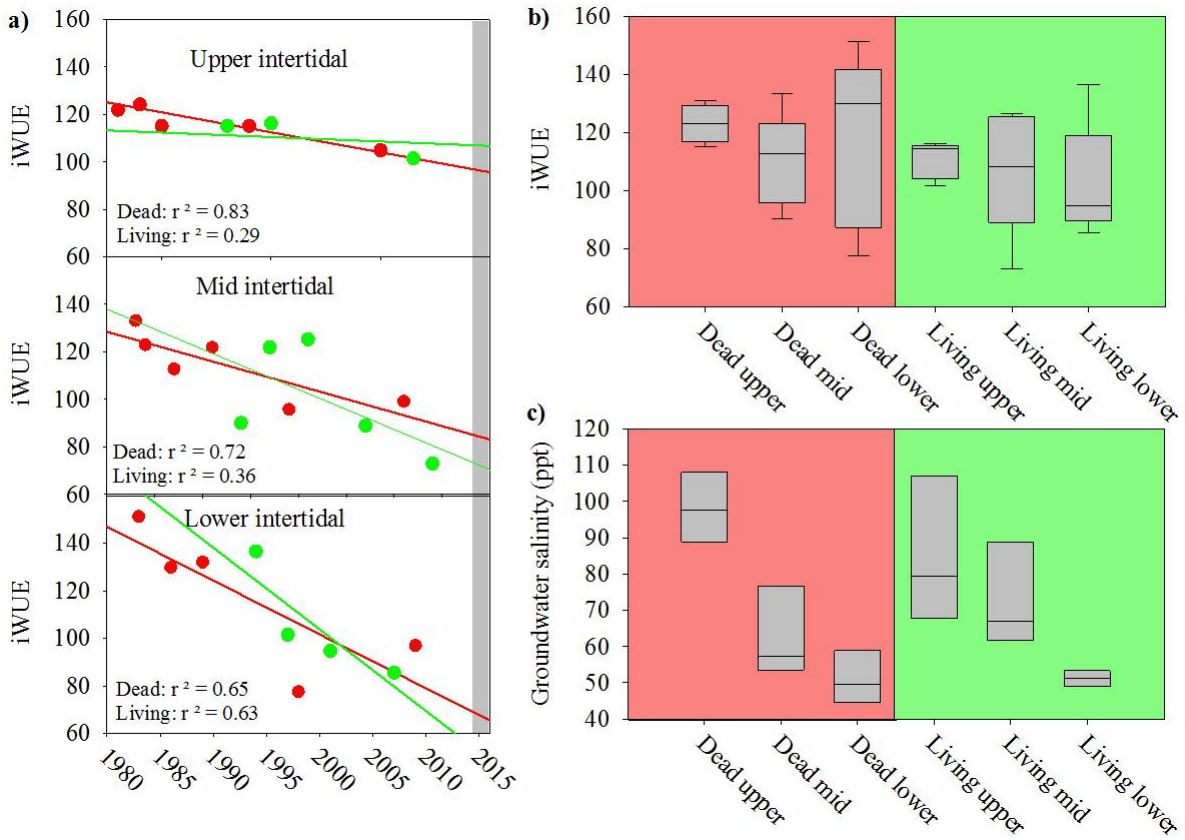

Figure 7. a) Changes to Water Use Efficiency (WUE) over time in wood samples collected from the upper, lower and mid intertidal zone in living (green) and dead (red) mangrove areas. The grey bar represents the mangrove dieback event. Error bars are not visible due to low error of individual samples. b) Box plot of water use efficiency in mangrove wood samples in dead and living mangrove areas in the upper, mid and lower intertidal zones. Sample size > 4 from each wood sample. The central horizontal line represents the median, the box represents the upper and lower quartiles, and the whiskers represent the maximum and minimum values. c) Box plot of groundwater salinity eight months post dieback event in dead and living mangrove areas in the upper, mid and lower intertidal zones. Sample size > 3 from each intertidal zone.

Normalised wood density values in the dead mangrove forest showed no change during the dieback event in the upper intertidal zone, but a decline in density values occurred in the mid and lower intertidal zones (Figure 8). In the living mangrove area, declines in wood density values occurred in the upper and mid intertidal zones during the mortality event, but no variation in density occurred in the lower intertidal zone (Figure 8).

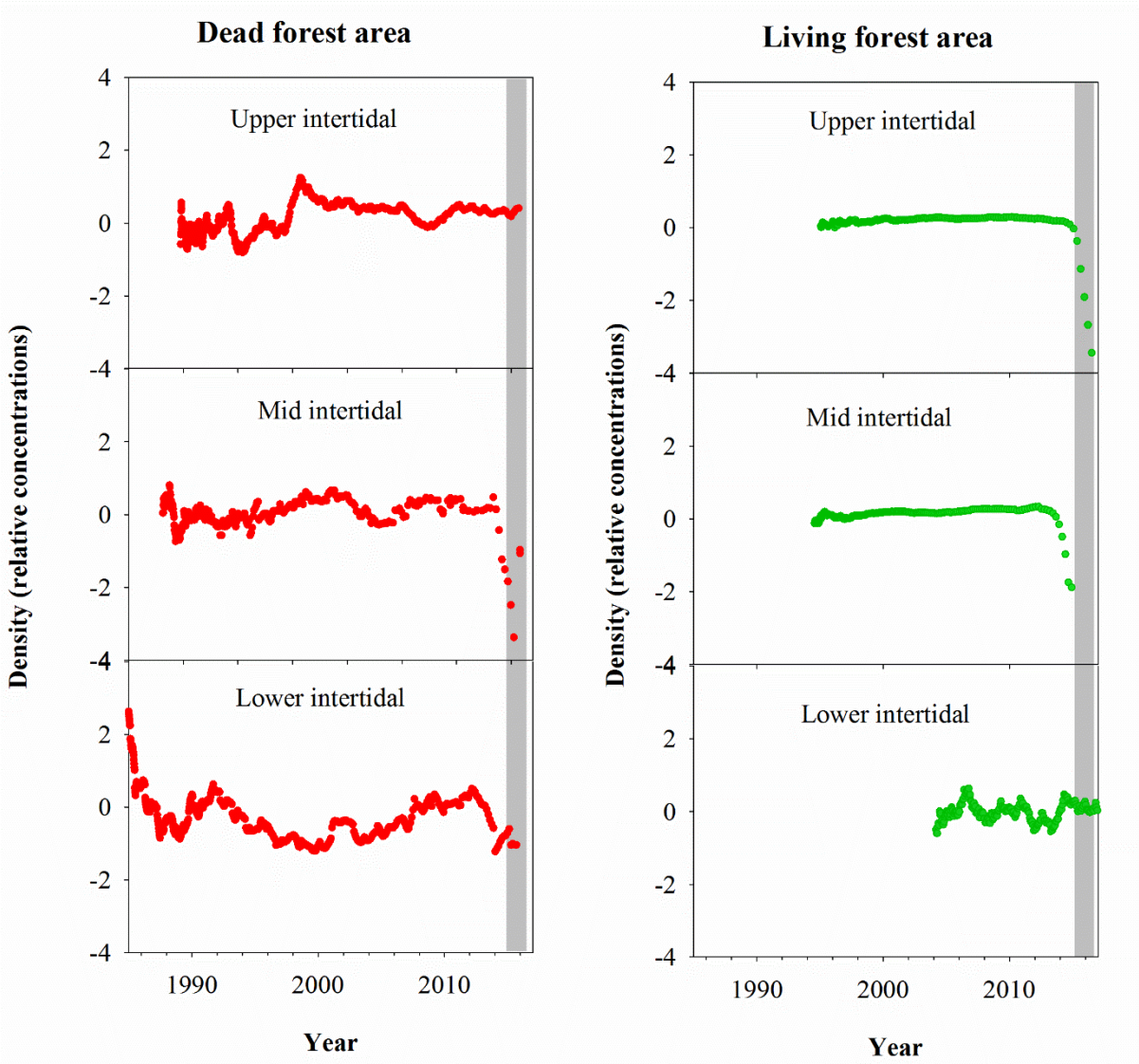

Figure 8. Normalised wood density (relative concentrations) in mangrove wood over time in living (green dots) and dead (red dots) mangrove areas of the Gulf of Carpentaria, Australia. The grey bar represents the time period of the dieback event.

Discussion

Evidence of differences in water availability between living and dead forest areas from dendrogeochemistry

Multiple lines of evidence from wood samples and sediment cores point to substantial differences in water availability between the dead and living mangrove areas. For example, Fe trends in wood (comparative Fe gain) and sediment samples (comparative Fe loss) (Figures 3, 5 and 6) within the dead mangrove zone, both suggest the mobilisation of bioavailable Fe as Fe^{2+}.These observations are consistent with oscillations in sedimentary redox conditions, triggered by changes in water availability, promoting mobilisation of Fe - firstly as bioauthigenic pyrite is oxidised and yet again during the reduction of Fe(III) oxide species when conditions return to being predominantly anaerobic (Figure 9). Increased oxygen diffusion into sediments during the period of low water availability likely resulted in the oxidation of bioauthigenic pyrite, which transformed into aqueous and bioavailable Fe^{2+} (e.g. Figure 9.2a; Johnston et al. 2011). With further oxidation, Fe^{2+} would likely have transformed into solid-phase Fe(III)oxides (Figure 9.2b). Such Fe(III) oxides are highly reactive and thus any subsequent short-term reduction (e.g. due to tidal inundation) would also result in re-mobilization of Fe as Fe^{2+} (Figure 9.2c). The fact that these trends in Fe that were observed in wood and soil samples were not observed for other elements analyzed by Itrax, supports the hypothesis that Fe trends were likely related to pyrite oxidation / redox oscillations (Appendix 1 & 2).

The most probable cause for a shift from reducing to oxidising conditions in the sediment is a reduction in water content (Keene et al. 2014) associated with the intense El Niño of 2015/16 and associated low sea level and annual rainfall (Figure 2). Trends in wood density, mangrove growth rate and water use efficiency also reveal distinct differences in water availability between dead and living forest areas. Lower water availability in the dead mangrove forest area was also evident in lower plant growth rates and higher plant water use efficiency. Mangrove plant isotope data at the same sites from a study by Harada et al. (2020) also shows a similar trend with more enriched $\delta^{13}C$ values in the dead mangrove zone.

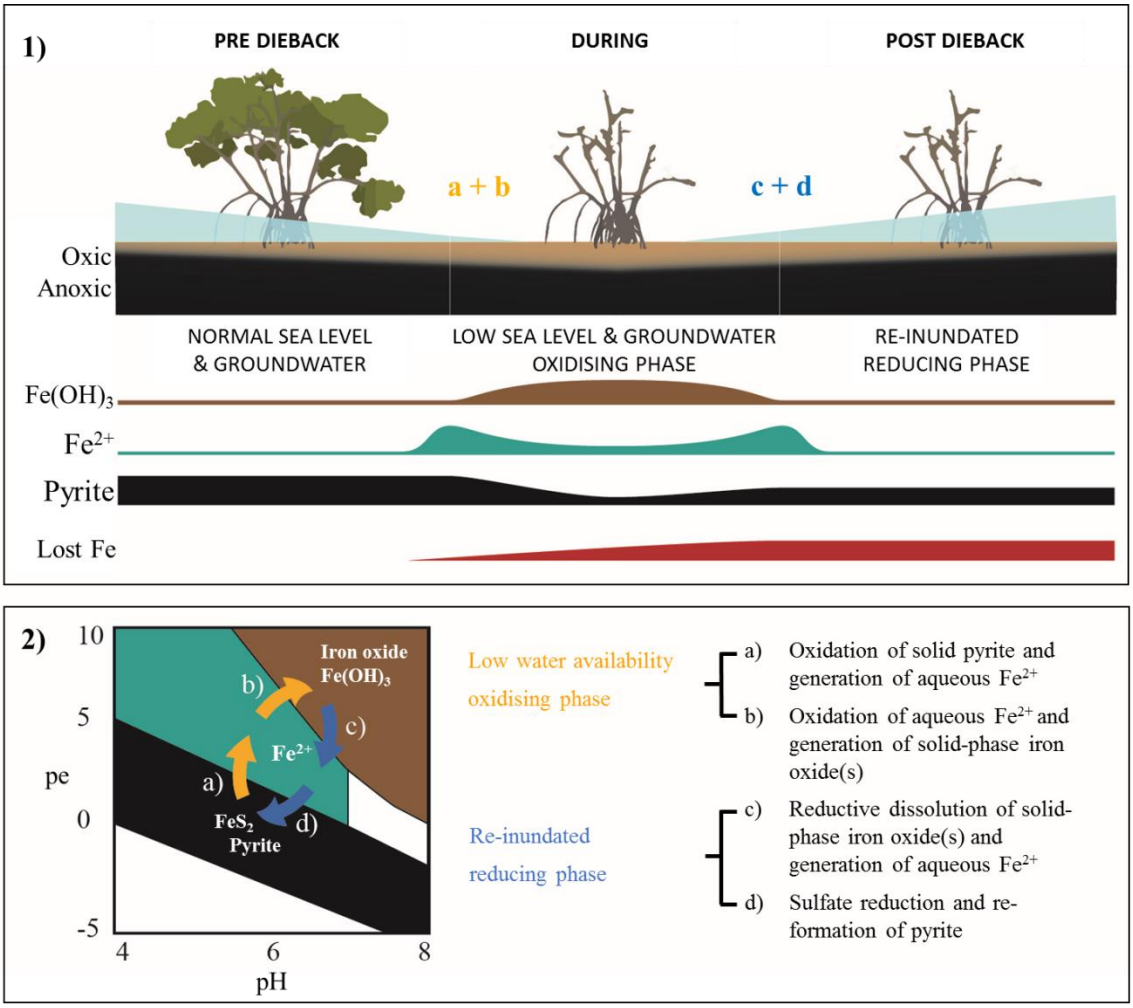

Figure 9. Conceptual diagram of Fe speciation under different sediment redox, pH conditions and 1) how speciation changes would be influenced by sea level and groundwater. Under initially elevated redox conditions due to low water availability 2) pyrite oxidation causes Fe transformation to (a) bioavailable Fe^{2+} and (b) particulate $Fe(OH)_3$, followed by eventual re-establishment of normal water availability / reducing conditions and (c) consequent reduction of $Fe(OH)_3$ and generation of Fe^{2+} followed by (d) sequestration of Fe(II) species via pyrite reformation.

Fe in wood

Elemental composition from wood samples suggest that the mangrove forest experienced sharp changes in sediment geochemistry during the dieback phase (Figure 3). This is consistent with low sea level and low rainfall/groundwater reducing soil water content, leading to oxidation of Fe sulphide minerals and release of Fe^{2+} (Figure 9.2a). The Fe peaks in the dead mangrove area at the time of tree mortality were 30 to 90 fold higher than baseline Fe (the mean Fe concentration in the sample prior to the dieback event).

In the living mangrove area, an Fe peak 25 fold higher than baseline Fe was observed in the upper intertidal zone (Figure 3). In the mid and lower intertidal areas of the living mangroves, Fe peaks were 4 and 3 fold higher than baseline respectively. In all living wood samples, Fe subsequently decreased after the dieback event, thereby suggesting that Fe in new wood

growth was diminished in association with a return to sustained reducing sediment conditions and a concomitant attenuation in porewater Fe^{2+} availability (Figure 9.2 d).

Records of all climate variables are in resolution of months, but the chronology of Fe (based on ^{14}C dates) is in years. We therefore used time lag analysis to examine relationships between climate variables and Fe over a two year period (Figure 4). Fe wood concentrations were significantly correlated with both rainfall and vapour pressure in the dead and living forest areas (Figure 4). However, because all climate variables were strongly correlated to each other, we cannot separate the relationships between individual climate drivers and Fe trends. We speculate that the combination of low availability of fresh groundwater and low sea level during the strong El Niño event of 2015/16 are key drivers of the sediment redox conditions, as reflected in wood Fe trends.

Considering the extreme increases in Fe concentrations observed in the wood samples during the dieback event, it is plausible that Fe toxicity could have contributed to mangrove mortality. However, we cannot fully test this hypothesis in this study and are unaware of research testing the toxicity of Fe in *A. marina* at highly elevated concentrations of bioavailable Fe^{2+}. Alongi, (2010) found that Fe toxicity occurred in some mangrove species at high concentrations (100 mmol m^2 d^{-1} of water-soluble Fe-EDTA) that were approximately 2 fold higher than the Fe supply for maximal growth. However, *A. marina* (the dominant species affected by the dieback at the study site) appear relatively resilient to high porewater Fe^{2+}. For example, Johnston et al. (2016) observed no *A. marina* mortality at porewater Fe^{2+} concentrations of 7-15 fold above normal in a mangrove forest impacted by acid sulfate drainage. Considering that other mangrove species are affected by Fe toxicity at twofold the optimal Fe availability, it is possible that a 30-90 fold increase in Fe could have been an additional stressor to mangroves already stressed by low water availability.

While our observations suggest complex sedimentary redox conditions occurred in dead zone mangrove sediments during the dieback event, linking drought and low sea level to porewater Fe concentrations requires further investigation. For example, crab burrows and root systems can induce conditions that increase O_2 diffusion into sediments and thus influence Fe^{2+} mobility over tidal cycles (Nielsen at al., 2003; Kirstensen et al., 2008). Localised Fe(III) oxide dissolution can also occur in redox / pH micro-niches and under suboxic conditions (Fabricius et al. 2014; Zhu et al. 2012). Further research on the mechanisms of bioavailable Fe release and the thresholds for Fe toxicities in *A. marina* is required to clearly understand the impacts of porewater Fe on mangrove forests.

Fe in sediments

Sediment cores also displayed considerable differences in down core Fe profiles between living and dead mangrove areas (Figure 5a and b). Normalized Fe concentrations were lower in the upper 1 m of sediments in the dead mangrove area compared to the living, but were very similar in sediments deeper than 1 m (Figure 5a and b). Similar trends were also observed in CRS (a proxy for pyrite, FeS_2) sediment core profiles, which have ~40 % lower FeS_2 concentrations in the dead mangroves in the upper 60 cm of the profile, in comparison to the living mangrove sediments (Figure 6). The fact that differences in down core trends in Fe are most prominent in the upper parts of the sediment cores is consistent with decreases in water availability being more confined to the upper parts of the sediment profile, whereas deeper sediments are more likely to have remained fully saturated.

Although mangrove sediment conditions are typically highly heterogeneous (Zhu et al. 2006, Zhu and Aller 2012), the sediment core results are broadly consistent with the wood data. The

apparent mobilisation of Fe (loss from sediment and uptake in wood) was not observed in other elements (Appendix 1 & 2). Sediment Fe:Mn ratios in Itrax data displayed no clear differences between living and dead mangrove areas. These similarities may be because the sediment cores were taken after the dieback period when sediment geochemistry conditions returned to normal. Trends in Mn in the wood samples (Appendix 1) also show no clear differences between living and dead forest areas and the Fe:Mn ratios in the wood Itrax data overwhelmingly reflect the Fe concentrations.

Sediment Fe losses, as implied by comparative Fe profiles (Figures 3, 4 & 6), also suggest a likely outwelling of Fe to the ocean. We estimate Fe outwelling by comparing FeS_2 concentrations in living and dead mangrove sediment cores based on the assumptions that (1) all Fe was originally in the form of FeS_2 and (2) tree Fe uptake is a minor loss pathway. The losses of Fe from the dead mangrove sediment would be equivalent to 87±163 mmol m^2 d^{-1}. The replication of CRS sediment cores (n = 4) greatly limits the accuracy of our estimates. However, these fluxes are remarkably similar to short-term porewater-derived dissolved Fe fluxes (79±75 mmol m^2 d^{-1}) estimated for a healthy temperate saltmarsh/mangrove system (Holloway et al. 2018), and provides some comparative restraint for our estimates.

If our sediment cores in dead and living mangroves were representative of changes within the entire dieback area (7400 ha), then total Fe losses from the dieback event could be equivalent to 87±163 Gg Fe. This loss is equivalent to 12 – 50% of global annual Fe inputs to the surface ocean from aerosols (Jickells et al. , Fung et al. 2000, Elrod et al. 2004). Since the surface ocean can be Fe limited, the consequences of Fe outwelling from this dieback event of such a magnitude may have had an effect on productivity in the Gulf of Carpentaria.

Wood density, growth trends and water use efficiency

Clear decreases in normalised wood density were observed during the mangrove mortality event (Figure 8). Similar to trends in wood Fe, the wood density values in the living and dead forest areas were correlated to climatic indicators (Appendix 3). In *A. marina* trees, the observed decreases in wood density likely indicates decreased growth, however the annual scale resolution of ^{14}C ages prevented detection of this short term change in our growth rate data. These clear decreases in wood density prior to tree mortality are therefore an indication of stress since decreased growth rates of mangroves can be associated with decreased water availability (Verheyden et al. 2005, Schmitz et al. 2006, Santini et al. 2013) which is also directly related to increased salinity. Low rainfall conditions and increased temperatures increase both evaporation and evapotranspiration while reducing freshwater inputs (Medina and Francisco 1997, Hoppe-Speer et al. 2013).

Interestingly, no decrease in density was observed in the upper intertidal area of the dead mangroves (Figure 8), despite the clear increase in Fe during the dieback in this tree (Figure 3). This suggests that no change in growth occurred prior to tree mortality, implying rapid mortality in this case. The upper intertidal area of the dead mangroves may have been living at the limit of its tolerance range for water availability or salinity prior to the dieback, as suggested by extremely high groundwater salinities in the upper intertidal areas of dead and living mangrove forests eight months post dieback event (Figure 7c). No decrease in wood density was observed in the lower intertidal area of the living mangroves, which is consistent with both variation in concentration of Fe and tree growth rate data. Together, these data suggest that the lower intertidal area of the living mangroves was not exposed to the same conditions during the dieback event as areas in the dead mangroves higher in the intertidal zone (Figures 3, 8 & 9). These results suggest a gradient of water availability, from extremely

low availability at the upper intertidal zone of the dead mangrove area to high/optimal availability at the lower intertidal zone of the living mangrove area. Since the elevation profiles are similar in the dead and living mangrove areas in the lower and mid intertidal areas (Figure 1), it is possible that the difference in Fe trends between the mangrove areas are associated with the influence of regional groundwater flows on sedimentary redox conditions.

Mean growth rates of trees in living (4.4 ± 3.6 mm yr^{-1}) and dead (5.3 ± 3.5 mm yr^{-1}) mangrove areas are similar to rates measured by Santini et al., (2013) in *A. marina* in arid Western Australia (4.1 to 5.3 mm yr^{-1}). However, there was ~10 fold greater variability because samples were collected from the upper, mid and lower intertidal zone, while Santini et al. (2012) sampled from the lower intertidal zone only. De-trended growth rate data showed no consistent differences in growth trends were identified between mangrove areas (Figure 8). The lower intertidal sample of the living mangroves grew more quickly during the dieback, which may suggest optimal conditions during this time. This may be due to increased nutrient availability due to litterfall inputs of organic matter from nearby stressed trees. All other sampled trees show no indication of reduced growth prior to or during the mortality event (Table 1). We suggest that climatic conditions drove very low growth rates during the dieback event, as indicated by wood density data (Figure 8) and previous studies that found low growth during droughts (Cook et al., 1977; Santini et al., 2013).

A significant difference in mean $\delta^{13}C$ and WUE between living or dead mangrove areas was observed in the upper intertidal zone (T-test, P = 0.02), but not in the mid or lower intertidal zones (Figure 7b). This is consistent with the zonation of mangrove mortality which occurred predominantly in the upper intertidal areas (Duke et al., 2017). The consistent decrease in WUE suggests that water availability has been increasing over time in all intertidal areas since the 1990's (Figure 7a). This is supported by generally increasing precipitation since 1980's (Figure 2), which enhanced mangrove areas in the Gulf of Carpentaria prior to this dieback event (Asbridge et al. 2016). Therefore, climatic conditions were initially favourable over the plants lifetime and trees may have been insufficiently acclimated to withstand drought and low soil water availability during the dieback. Overall, this highlights the important role of extreme climatic events counterbalancing mangrove responses to gradual climate trends (Harris et al. 2018).

Differences in water availability between living and dead forest areas

We have no data to determine if regional groundwater availability was greater in living forest areas than dead forest areas during the mangrove dieback. No significant difference was observed in groundwater salinities 8 months post dieback. However, under normal sea level conditions (i.e. when groundwater samples were collected), tidal inundation is likely to be the predominant driver of groundwater salinities rather than groundwater flows. Duke et al. (2017) and Harris et al. (2017) provide strong evidence that water availability in the Gulf of Carpentaria was extremely low prior to and during the dieback event. In this study we have been able to build on this work by exploring links between changes in sediment geochemistry and low water availability.

We eliminate elevation as a potential driver of water availability in living and dead forest areas. Tree mortality occurred even in the lower intertidal zone of the dead mangrove area which are at the same elevation as the lower intertidal zone of the living forest area (see

elevation DEM in Figure 1c). Since other potential water sources were comparable between the sites, differences in water availability were likely driven by groundwater availability. Groundwater flows have high spatial variability and have been demonstrated to be an important water source in mangroves from arid Australia. For example Stieglitz (2005) highlights that the interrelationships between confined and unconfined aquifers in the coastal zone can result in localised differences in groundwater flows. High resolution spatial analysis of groundwater salinities in living and dead forest areas during low sea level conditions would help to clarify how water sources may drive mangrove mortality.

Limitations

This study is inherently limited in its spatial extent. Thus, the differences in Fe between samples from living and dead mangrove areas may be due to causal factors beyond the scope of this study. However, the consistency of results from multiple methods and divergent sample types provides some confidence in the interpretation that recent changes in sediment geochemistry have occurred associated with extreme drought and low sea level events.

Our analysis benefited from the development of high precision ^{14}C dating of mangrove wood samples (with age uncertainties of 1-3 calendar years (1σ); see Table 1) that rely on atmospheric bomb ^{14}C content resulting from above-ground nuclear testing mostly in the late 1950's and early 1960's (Hua and Barbetti 2004a). The complexity in the wood development of *A. marina* creates uncertainties (Robert et al. 2011). *Avicennia marina* secondary growth is atypical, displaying consecutive bands of xylem and phloem which can result in multiple cambia (i.e. the tissue providing undifferentiated cells for the growth of plants) being simultaneously active (Schmitz et al., 2006; Robert et al., 2011). Furthermore, *A. marina* cambia display non-cylindrical or asymmetrical growth (Maxwell et al. 2018). These characteristics of *A. marina* atypical growth can influence our results as there is variation within each stem.

As younger wood grows on the exterior of the tree, errors associated with the estimated ages do not introduce uncertainty in the direction of trends but decrease the ability of finding correlated trends with climatic variables (Van Der Sleen et al. 2015). In spite of these uncertainties, the strong cross correlations displayed in Figure 4, with minimal time lag suggest that the dendrochronology results are robust, and that climate variability drives long-term Fe cycling in the coastal mangroves of the Gulf of Carpentaria.

Summary and Conclusions

Wood and sediment geochemical data from living and dead mangrove areas suggest there were substantive differences in their comparative sediment redox conditions during the dieback event. Climatic data and patterns in Fe concentrations in wood and sediment samples, suggest that sediment oxidation occurred in combination with unprecedented low sea levels and low rainfall. As the elevation of dead and living mangrove areas was very similar, we suggest that the differences in tree survival between areas were probably due to higher groundwater availability in the living site. Evidence of plant Fe uptake and losses of Fe from sediments are consistent with this hypothesized Fe mobilization associated with low water availability in sediments. The dieback event was likely a period of transitioning redox states in a heterogeneous sediment matrix, which resulted in areas of mangrove sediments with low water availability combined with porewaters enriched in bioavailable Fe (Figure 9).

Our data suggest that extremely low water availability drove the mangrove dieback. However, mangrove dieback may also be associated with increased concentrations of bioavailable Fe^{2+} in porewaters that occurred during this time of low water availability. Estimated losses of Fe from sediments were consistent with the observed plant uptake and suggest Fe mobilisation due to sediment oxidation (and subsequent reduction). This Fe mobilisation may also have led to significant Fe inputs to the ocean.

This study supports climate observations suggesting that the Gulf of Carpentaria dieback was strongly driven by an extreme ENSO event (Harris et al. 2017). Climate change is increasing the intensity of ENSO events and climate extremes (Lee and McPhaden 2010, Cai et al. 2014, Freund et al. 2019) and increasing sea level variability (Widlansky et al. 2015), which is impacting on mangrove forests in arid coastlines (Lovelock et al. 2017). This study therefore builds on the premise that the dieback event was associated with climate change (Harris et al. 2018). Further research is necessary to understand the role of Fe in tree mortalities, to constrain potential Fe losses to the ocean and from sediments and to understand thresholds for Fe toxicities in *A.marina*.

Acknowledgements

JZ Sippo acknowledges funding support and access to ANSTO facilities from AINSE which made this project possible. We would like to thank Jocelyn Turnbull for giving us permission to use atmospheric ^{14}C data extended to 2017 from Baring Head (Wellington). The study was funded by the Australian Research Council (DE150100581, DP180101285, DE160100443, DP150103286 and LE140100083).

References

Alber, M., E. M. Swenson, S. C. Adamowicz and I. A. Mendelssohn (2008). "Salt Marsh Dieback: An overview of recent events in the US." *Estuar. Coast. Shelf Sci.* **80**(1): 1-11.

Alongi, D. M. (2015). "The Impact of Climate Change on Mangrove Forests." *Current Climate Change Reports* **1**(1): 30-39.

Asbridge, E., R. Bartolo, C. M. Finlayson, R. M. Lucas, K. Rogers and C. D. Woodroffe (2019). "Assessing the distribution and drivers of mangrove dieback in Kakadu National Park, northern Australia." *Estuar. Coast. Shelf Sci.* **228**: 106353.

Asbridge, E., R. Lucas, C. Ticehurst and P. Bunting (2016). "Mangrove response to environmental change in Australia's Gulf of Carpentaria." *Ecology and evolution* **6**(11): 3523-3539.

Barbier, E. B., S. D. Hacker, C. Kennedy, E. W. Koch, A. C. Stier and B. R. Silliman (2011). "The value of estuarine and coastal ecosystem services." *Ecol. Monogr.* **81**(2): 169-193.

Bronk Ramsey, C. (2008). “Deposition models for chronological records.” *Quat. Sci. Rev.* **27**: 42-60.

Brookhouse, M. (2006). "Eucalypt dendrochronology: past, present and potential." *Aust. J. Bot.* **54**(5): 435-449.

Burdige, D. J. (2011). "Estuarine and coastal sediments – coupled biogeochemical cycling." *Treatise on Estuarine and Coastal Science* **5**: 279-316.

Bureau of Meteorology (2019). "Climate data online." Retrieved 12/08/19, from http://www.bom.gov.au/climate/data/.

Burton, E. D., R. T. Bush and L. A. Sullivan (2006). "Sedimentary iron geochemistry in acidic waterways associated with coastal lowland acid sulfate soils." *Geochim. Cosmochim. Acta* **70**(22): 5455-5468.

Burton, E. D., L. A. Sullivan, R. T. Bush, S. G. Johnston and A. F. Keene (2008). "A simple and inexpensive chromium-reducible sulfur method for acid-sulfate soils." *Appl. Geochem.* **23**(9): 2759-2766.

Cai, W., S. Borlace, M. Lengaigne, P. van Rensch, M. Collins, G. Vecchi, A. Timmermann, A. Santoso, M. J. McPhaden, L. Wu, M. H. England, G. Wang, E. Guilyardi and F.-F. Jin

(2014). "Increasing frequency of extreme El Niño events due to greenhouse warming." *Nature Climate Change* **4**: 111.

Donato, D. C., J. B. Kauffman, D. Murdiyarso, S. Kurnianto, M. Stidham and M. Kanninen (2011). "Mangroves among the most carbon-rich forests in the tropics." *Nature Geosci* **4**(5): 293-297.

Elrod, V. A., W. M. Berelson, K. H. Coale and K. S. Johnson (2004). "The flux of iron from continental shelf sediments: A missing source for global budgets." *Geophys. Res. Lett.* **31**(12).

Fabricius, A.-L., Duester, L., Ecker, D., Ternes, T.A., 2014. “New Microprofiling and Micro Sampling System for Water Saturated Environmental Boundary Layers”. *Environmental Science & Technology*, **48**(14): 8053-8061.

Farquhar, G., K. Hubick, A. Condon and R. Richards (1989). Carbon isotope fractionation and plant water-use efficiency. *Stable isotopes in ecological research*, Springer**:** 21-40.

Farquhar, G. and R. Richards (1984). "Isotopic composition of plant carbon correlates with water-use efficiency of wheat genotypes." *Funct. Plant Biol.* **11**(6): 539-552.

Fink, D., M. Hotchkis, Q. Hua, G. Jacobsen, A. M. Smith, U. Zoppi, D. Child, C. Mifsud, H. van der Gaast and A. Williams (2004). "The antares AMS facility at ANSTO." *Nuclear Instruments and Methods in Physics Research Section B: Beam Interactions with Materials and Atoms* **223**: 109-115.

Freund, M. B., B. J. Henley, D. J. Karoly, H. V. McGregor, N. J. Abram and D. Dommenget (2019). "Higher frequency of Central Pacific El Niño events in recent decades relative to past centuries." *Nature Geoscience* **12**(6): 450-455.

Fung, I. Y., S. K. Meyn, I. Tegen, S. C. Doney, J. G. John and J. K. Bishop (2000). "Iron supply and demand in the upper ocean." *Global Biogeochem. Cycles* **14**(1): 281-295.

Google Earth (2019). "Karumba, Qld, Australia". Digital Globe

Gilman, E. L., J. Ellison, N. C. Duke and C. Field (2008). "Threats to mangroves from climate change and adaptation options: A review." *Aquat. Bot.* **89**(2): 237-250.

Gregory, B. R. B., R. T. Patterson, E. G. Reinhardt, J. M. Galloway and H. M. Roe (2019). "An evaluation of methodologies for calibrating Itrax X-ray fluorescence counts with ICP-MS concentration data for discrete sediment samples." *Chemical Geology* **521**: 12-27.

Hamilton, S. E. and D. Casey (2016). "Creation of a high spatio-temporal resolution global database of continuous mangrove forest cover for the 21st century (CGMFC-21)." *Global Ecol. Biogeogr.* **25**(6): 729-738.

Harada, Y., R. M. Connolly, B. Fry, D. T. Maher, J. Z. Sippo, L. C. Jeffrey, A. J. Bourke and S. Y. Lee (2020). "Stable isotopes track the ecological and biogeochemical legacy of mass mangrove forest dieback in the Gulf of Carpentaria, Australia." *Biogeosciences Discuss.* **2020**: 1-32.

Harris, R. M. B., L. J. Beaumont, T. R. Vance, C. R. Tozer, T. A. Remenyi, S. E. Perkins-Kirkpatrick, P. J. Mitchell, A. B. Nicotra, S. McGregor, N. R. Andrew, M. Letnic, M. R. Kearney, T. Wernberg, L. B. Hutley, L. E. Chambers, M. S. Fletcher, M. R. Keatley, C. A. Woodward, G. Williamson, N. C. Duke and D. M. J. S. Bowman (2018). "Biological responses to the press and pulse of climate trends and extreme events." *Nature Climate Change* **8**(7): 579-587.

Harris, T., P. Hope, E. Oliver, R. Smalley, J. Arblaster, N. Holbrook, N. Duke, K. Pearce, K. Braganza and N. Bindoff (2017). Climate drivers of the 2015 Gulf of Carpentaria mangrove dieback. N. E. S. Program. Earth System and Climate Change Hub Technical Report 2, Australian Government.

Hevia, A., R. Sánchez-Salguero, J. J. Camarero, A. Buras, G. Sangüesa-Barreda, J. D. Galván and E. Gutiérrez (2018). "Towards a better understanding of long-term wood-chemistry variations in old-growth forests: A case study on ancient Pinus uncinata trees from the Pyrenees." *Sci. Total Environ.* **625**: 220-232.

Holloway, C. J., I. R. Santos and A. L. Rose (2018). "Porewater inputs drive Fe redox cycling in the water column of a temperate mangrove wetland." *Estuar. Coast. Shelf Sci.* **207**: 259-268.

Holloway, C. J., I. R. Santos, D. R. Tait, C. J. Sanders, A. L. Rose, B. Schnetger, H.-J. Brumsack, P. A. Macklin, J. Z. Sippo and D. T. Maher (2016). "Manganese and iron release from mangrove porewaters: a significant component of oceanic budgets?" *Mar. Chem.* **184**: 43-52.

Hoppe-Speer, S. C. L., J. B. Adams and A. Rajkaran (2013). "Response of mangroves to drought and non-tidal conditions in St Lucia Estuary, South Africa." *Afr. J. Aquat. Sci.* **38**(2): 153-162.

Hua, Q. and M. Barbetti (2004a). "Review of tropospheric bomb 14C data for carbon cycle modeling and age calibration purposes." *Radiocarbon* **46**(3): 1273-1298.

Hua, Q., M. Barbetti, U. Zoppi, D. Fink, M. Watanasak and G. E. Jacobsen (2004b). "Radiocarbon in tropical tree rings during the Little Ice Age." *Nuclear Instruments and Methods in Physics Research Section B: Beam Interactions with Materials and Atoms* **223**: 489-494.

Hua, Q., G. E. Jacobsen, U. Zoppi, E. M. Lawson, A. A. Williams, A. M. Smith and M. J. McGann (2001). "Progress in radiocarbon target preparation at the ANTARES AMS Centre." *Radiocarbon* **43**(2A): 275-282.

Hunt, J. E., I. W. Croudace and S. E. MacLachlan (2015). Use of calibrated ITRAX XRF data in determining turbidite geochemistry and provenance in Agadir Basin, Northwest African passive margin. *Micro-XRF Studies of Sediment Cores*, Springer**:** 127-146.

Jickells, T. and L. Spokes The biogeochemistry of iron in seawater, edited by: DR Turner, KH, Wiley, Chichester, UK.

Johnston, S. G., A. F. Keene, R. T. Bush, E. D. Burton, L. A. Sullivan, L. Isaacson, A. E. McElnea, C. R. Ahern, C. D. Smith and B. Powell (2011). "Iron geochemical zonation in a tidally inundated acid sulfate soil wetland." *Chem. Geol.* **280**(3): 257-270.

Johnston, S. G., B. Morgan and E. D. Burton (2016). "Legacy impacts of acid sulfate soil runoff on mangrove sediments: Reactive iron accumulation, altered sulfur cycling and trace metal enrichment." *Chem. Geol.* **427**: 43-53.

Jones, D. A., W. Wang and R. Fawcett (2009). "High-quality spatial climate data-sets for Australia." *Australian Meteorological and Oceanographic Journal* **58**(4): 233.

Keene, A. F., S. G. Johnston, R. T. Bush, E. D. Burton, L. A. Sullivan, M. Dundon, A. E. McElnea, C. D. Smith, C. R. Ahern and B. Powell (2014). "Enrichment and heterogeneity of trace elements at the redox-interface of Fe-rich intertidal sediments." *Chem. Geol.* **383**: 1-12.

Kristensen, E., S. Bouillon, T. Dittmar and C. Marchand (2008). "Organic carbon dynamics in mangrove ecosystems: A review." *Aquatic Botany* **89**(2): 201-219.

Lee, T. and M. J. McPhaden (2010). "Increasing intensity of El Niño in the central-equatorial Pacific." *Geophys. Res. Lett.* **37**(14).

Lovelock, C. E., D. R. Cahoon, D. A. Friess, G. R. Guntenspergen, K. W. Krauss, R. Reef, K. Rogers, M. L. Saunders, F. Sidik and A. Swales (2015). "The vulnerability of Indo-Pacific mangrove forests to sea-level rise." *Nature*.

Lovelock, C. E., I. C. Feller, R. Reef, S. Hickey and M. C. Ball (2017). "Mangrove dieback during fluctuating sea levels." *Scientific Reports* **7**(1): 1680.

Marchand, C., J. M. Fernandez and B. Moreton (2016). "Trace metal geochemistry in mangrove sediments and their transfer to mangrove plants (New Caledonia)." *Science of the Total Environment* **562**: 216-227.

Maxwell, J. T., G. L. Harley and A. F. Rahman (2018). "Annual Growth Rings in Two Mangrove Species from the Sundarbans, Bangladesh Demonstrate Linkages to Sea-Level Rise and Broad-Scale Ocean-Atmosphere Variability." *Wetlands* **38**(6): 1159-1170.

McKee, K. L., I. A. Mendelssohn and M. D. Materne (2004). "Acute salt marsh dieback in the Mississippi River deltaic plain: a drought-induced phenomenon?" *Global Ecol. Biogeogr.* **13**(1): 65-73.

Medina, E. and M. Francisco (1997). "Osmolality and δ 13 C of leaf tissues of mangrove species from environments of contrasting rainfall and salinity." *Estuar. Coast. Shelf Sci.* **45**(3): 337-344.

Nguyen, H. T., P. Meir, L. Sack, J. R. Evans, R. S. Oliveira and M. C. Ball (2017). "Leaf water storage increases with salinity and aridity in the mangrove Avicennia marina: integration of leaf structure, osmotic adjustment and access to multiple water sources." *Plant, Cell Environ.* **40**(8): 1576-1591.

Nielsen, O. I., E. Kristensen and D. J. Macintosh (2003). "Impact of fiddler crabs (Uca spp.) on rates and pathways of benthic mineralization in deposited mangrove shrimp pond waste." *Journal of Experimental Marine Biology and Ecology* **289**(1): 59-81.

Ogburn, M. B. and M. Alber (2006). "An investigation of salt marsh dieback in Georgia using field transplants." *Estuaries and Coasts* **29**(1): 54-62.

Queensland Government (2019). "QldGlobe." Sourced from https://qldglobe.information.qld.gov.au.

Richards, D. R. and D. A. Friess (2016). "Rates and drivers of mangrove deforestation in Southeast Asia, 2000–2012." *Proceedings of the National Academy of Sciences* **113**(2): 344-349.

Robert, E. M., N. Schmitz, J. A. Okello, I. Boeren, H. Beeckman and N. Koedam (2011). "Mangrove growth rings: fact or fiction?" *Trees* **25**(1): 49-58.

Santini, N. S., Q. Hua, N. Schmitz and C. E. Lovelock (2013). "Radiocarbon dating and wood density chronologies of mangrove trees in arid Western Australia." *PloS one* **8**(11): e80116.

Santini, N. S., N. Schmitz and C. E. Lovelock (2012). "Variation in wood density and anatomy in a widespread mangrove species." *Trees* **26**(5): 1555-1563.

Schmitz, N., A. Verheyden, H. Beeckman, J. G. KAIRO and N. Koedam (2006). "Influence of a salinity gradient on the vessel characters of the mangrove species Rhizophora mucronata." *Ann. Bot.* **98**(6): 1321-1330.

Silliman, B. R., J. Van De Koppel, M. D. Bertness, L. E. Stanton and I. A. Mendelssohn (2005). "Drought, snails, and large-scale die-off of southern US salt marshes." *Science* **310**(5755): 1803-1806.

Sippo, J. Z., C. E. Lovelock, I. R. Santos, C. J. Sanders and D. T. Maher (2018). "Mangrove mortality in a changing climate: An overview." *Estuar. Coast. Shelf Sci.* **215**: 241-249.

Sippo, J. Z., D. T. Maher, K. G. Schulz, C. J. Sanders, A. McMahon, J. Tucker and I. R. Santos (2019). "Carbon outwelling across the shelf following a massive mangrove dieback in Australia: Insights from radium isotopes." *Geochimica et Cosmochimica Acta* **253**: 142-158.

Sippo, J. Z., C.J. Sanders, I. R. Santos, L.C. Jeffrey, M. Call, Y. Harada, K. Maguire, D. Brown, S.R. Conrad and D. T. Maher (2019). " Coastal carbon cycle changes following mangrove loss”. .*Limnology and Oceanography*. DOI:10.1002/lno.11476

Turner, J. N., N. Holmes, S. R. Davis, M. J. Leng, C. Langdon and R. G. Scaife (2015). "A multiproxy (micro-XRF, pollen, chironomid and stable isotope) lake sediment record for the Lateglacial to Holocene transition from Thomastown Bog, Ireland." *Journal of Quaternary Science* **30**(6): 514-528.

Van Breemen, N. (1988). Redox Processes of Iron and Sulfur Involved in the Formation of Acid Sulfate Soils. *Iron in Soils and Clay Minerals*. J. W. Stucki, B. A. Goodman and U. Schwertmann. Dordrecht, Springer Netherlands**:** 825-841.

Van Der Sleen, P., P. Groenendijk, M. Vlam, N. P. Anten, A. Boom, F. Bongers, T. L. Pons, G. Terburg and P. A. Zuidema (2015). "No growth stimulation of tropical trees by 150 years of CO 2 fertilization but water-use efficiency increased." *Nature geoscience* **8**(1): 24.

Verheyden, A., F. De Ridder, N. Schmitz, H. Beeckman and N. Koedam (2005). "High-resolution time series of vessel density in Kenyan mangrove trees reveal a link with climate." *New Phytol.* **167**(2): 425-435.

Widlansky, M. J., A. Timmermann and W. Cai (2015). "Future extreme sea level seesaws in the tropical Pacific." *Science Advances* **1**(8): e1500560.

Zhu, Q. and R. C. Aller (2012). "Two-dimensional dissolved ferrous iron distributions in marine sediments as revealed by a novel planar optical sensor." *Mar. Chem.* **136**: 14-23.

Zhu, Q., R. C. Aller and Y. Fan (2006). "Two-dimensional pH distributions and dynamics in bioturbated marine sediments." *Geochim. Cosmochim. Acta* **70**(19): 4933-4949.

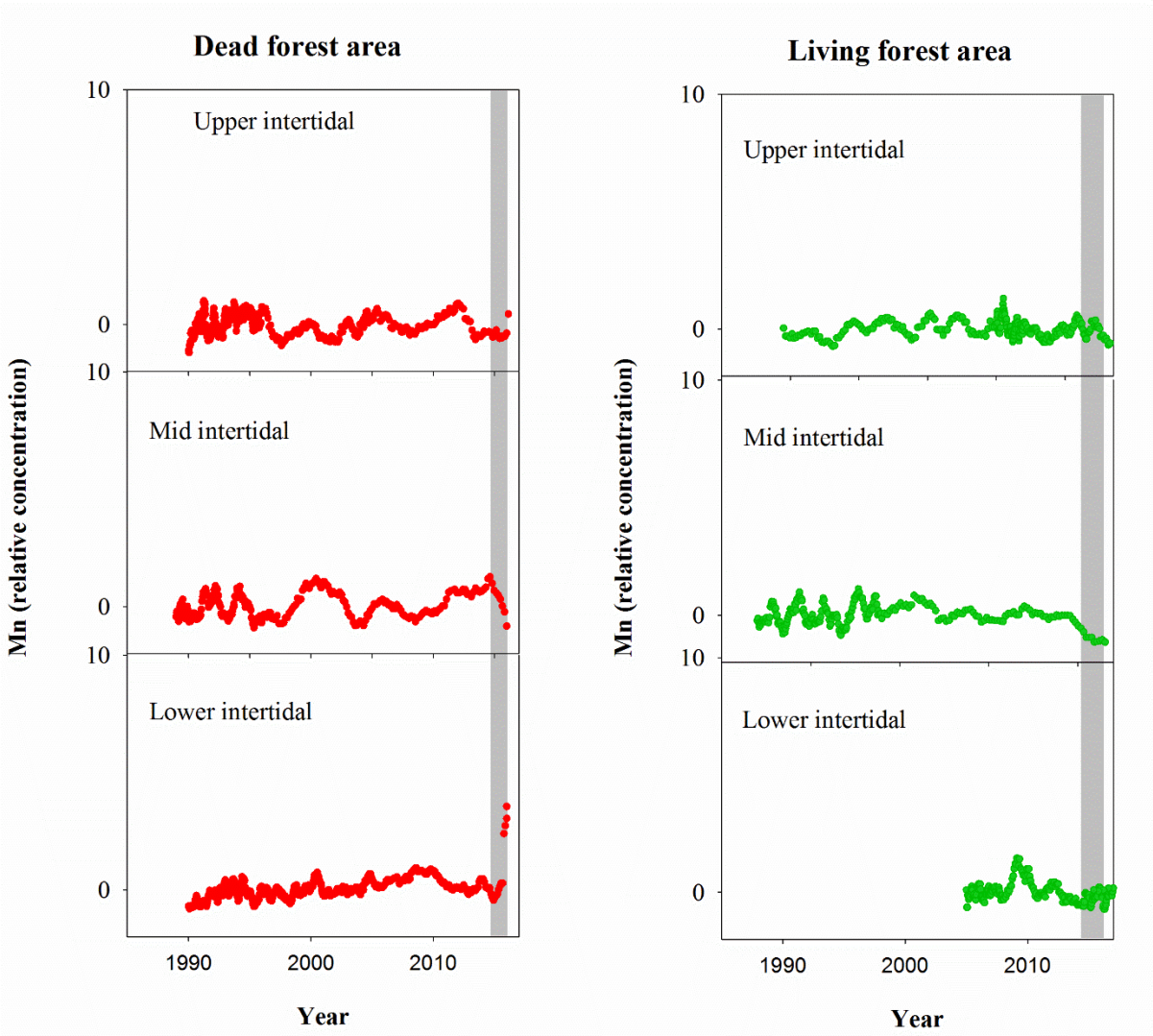

Appendix 1. Normalized Mn relative concentrations in mangrove wood over time in living (green dots) and dead (red dots) from upper, mid and lower intertidal areas of mangroves of the Gulf of Carpentaria, Australia. Grey areas indicate the dieback event.

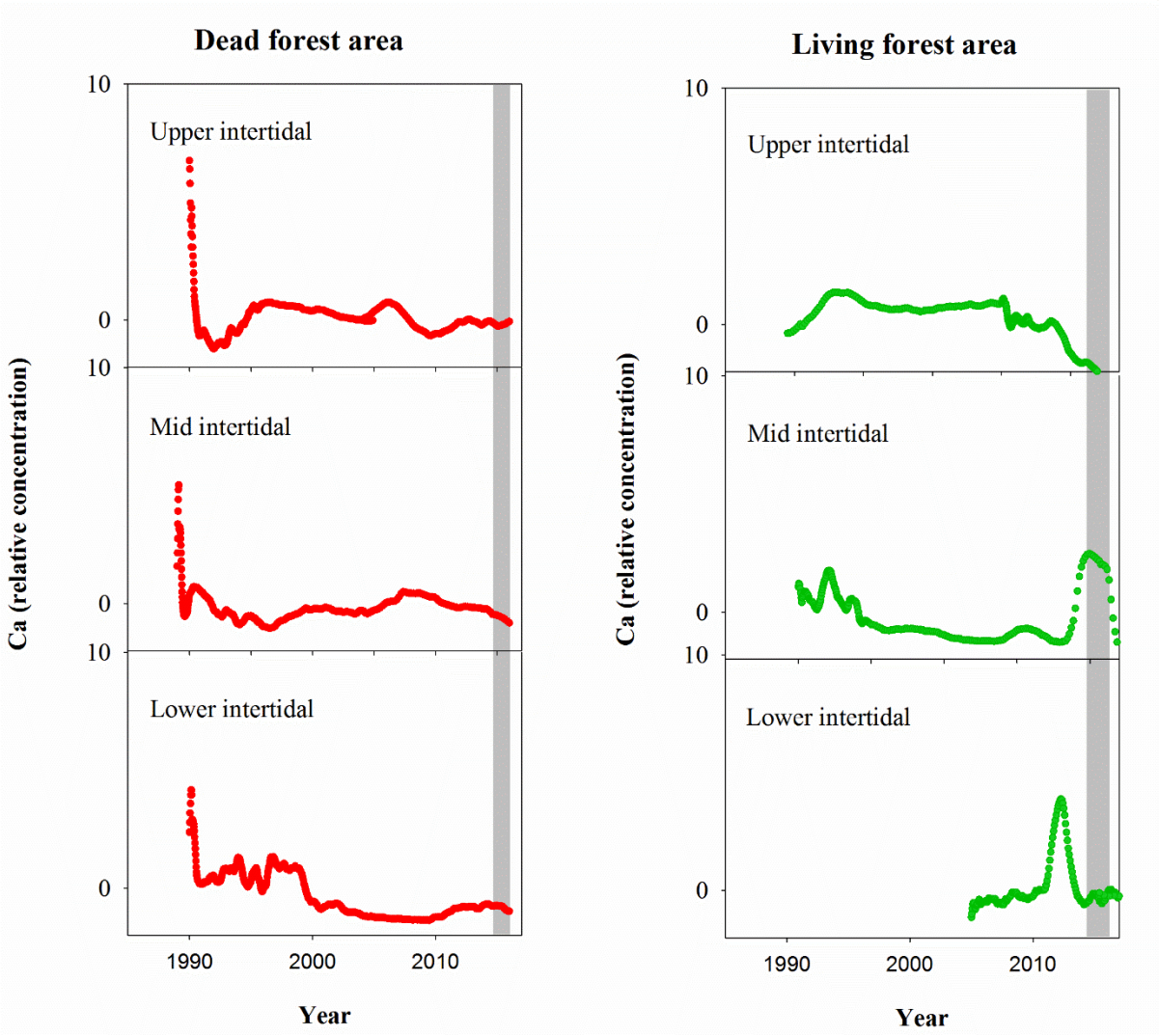

Appendix 2. Normalized Ca relative concentrations in mangrove wood over time in living (green dots) and dead (red dots) from upper, mid and lower intertidal areas of mangroves of the Gulf of Carpentaria, Australia. Grey areas indicate the dieback event.

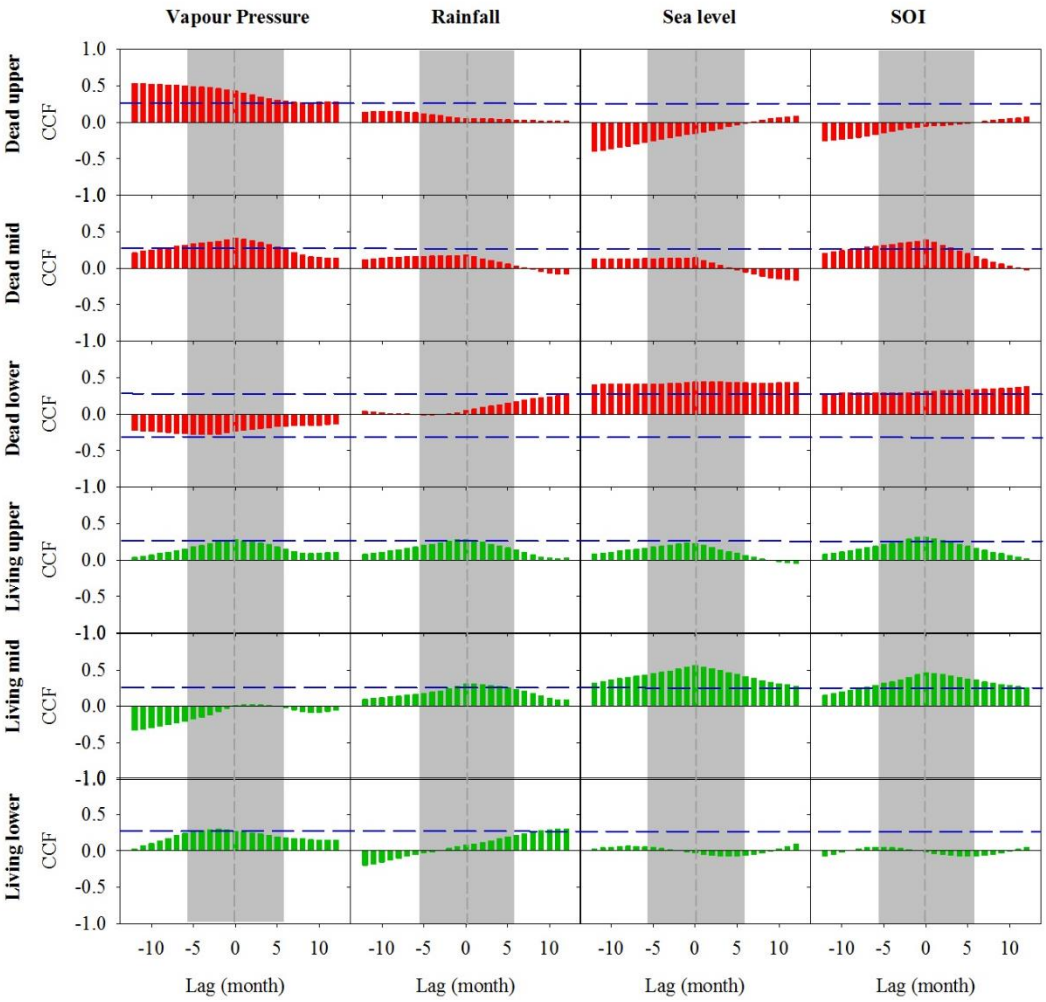

Appendix 3. Cross correlation function (CCF) analysis of the relationship between wood density and climate data over time at one month resolution over a 12 month period prior and post dieback. Wood samples are from the upper, mid and lower intertidal zones of the dead (red) and living (green) mangrove areas. Blue horizontal dashed lines indicate P< 0.01 with n=125. Grey dashed vertical lines at zero lag indicate dieback period.